Crisis-induced chaos in Josephson tunnel junctions

1992 J. Phys.: Condens. Matter 4 4829

(http://iopscience.iop.org/0953-8984/4/20/010)

J. Phys.: Condens. Matter 4 (1992) 4829–4838. Printed in the UK

Crisis-induced chaos in Josephson tunnel junctions

G Ambika†
Department of Physics, Cochin University of Science and Technology, Kochi-682 022, India

Received 15 May 1991, in final form 4 November 1991

Abstract. An analysis of Josephson tunnel junctions based on the RSJ model with non-linear damping reveals that crisis is the major mechanism that brings about chaos in the system. Details regarding the transition to chaos from zero-voltage steps and non-zero-voltage steps are discussed. The effect of a DC bias in the transition scenario as well as the evolution of the fractal basin boundaries near the crisis regions are studied.

1. Introduction

The non-linear nature of the dynamics underlying Josephson junctions is known to be responsible for the noise-rise phenomena or chaotic behaviour observed in them (Huberman and Crutchfield 1979, Huberman *et al* 1980). As such, these junctions have been the focus of much activity and research relating to studies in chaos and non-linear systems (Gwinn and Westervelt 1986, Cicogna 1987, 1988, Jing 1989, Yao *et al* 1990). Most of the earlier studies were based on the resistively shunted junction (RSJ) model with a constant resistance (D'Humieres *et al* 1982, Kautz and Monaco 1985, Iansiti *et al* 1985). However, of late, a modified model, in which the shunted resistance depends inversely on the voltage leading to quadratic damping in the system (called quadratic RSJ or QRSJ) has been proposed (Pedersen and Saermark 1973, Bartuccelli *et al* 1986). This takes into account the non-linear nature of the I–V characteristics, especially in the case of tunnel junctions at finite temperatures. In addition to reproducing most of the salient features of the RSJ model, the QRSJ has several interesting results to its credit.

In our recent works, we have pointed out that the quadratic nature of the damping can introduce instabilities and transients in the response of the system to RF driving (Ambika and Babu Joseph 1990, Ambika *et al* 1991) and have reformulated the problem using a Hamiltonian approach (Ambika 1990). The Melnikov method of analysis has been found to predict the lowest threshold for chaos in the system (Bartuccelli *et al* 1986, Yao *et al* 1990). The two different types of oscillatory modes as well as the two types of chaos exhibited by QRSJ have been discussed by Xiao and Yao (1989). However, the details regarding the mechanism of onset of chaos and the dependence of the threshold on all the parameters of the problem are still not completely analysed.

In the present work, we try to fill this lacuna by carrying out a detailed parameter space analysis with and without DC bias. Our numerical studies reveal that crisis is the

† On leave from: Department of Physics, Maharaja's College, Kochi-682 011, India.

0953-8984/92/204829 + 10 $04.50

major mechanism of onset of chaos, even though period doubling occurs in a narrow region. For small values of the driving frequency, chaos is induced by a reverse boundary crisis while on the high-frequency side, at high amplitudes of the driving force, large-amplitude oscillatory modes with zero average voltage undergo period doubling followed by an interior crisis. This leads to a chaotic state where the system randomly shuttles between different voltage steps that have become unstable.

In section 2, we present the necessary details regarding the model. Section 3 deals with the details of the parameter space analysis both with and without a DC bias. The stable periodic modes, which are of course the most relevant ones as far as practical circuits with Josephson junctions are concerned, are discussed in section 4. Section 5 describes how crisis brings about chaos in the present model. Our concluding remarks and a comparison of this model with the usual RSJ are given in section 6.

2. The QRSJ model for Josephson tunnel junctions

The dynamics of an active S–I–S tunnel junction is described by a two-fluid model where the current through the junction can be written as (Harris 1974),

$$i(t) = I_1 \sin\theta + i_2 + i_3 \cos\theta \tag{2.1}$$

and the voltage across the junction is

$$v(t) = \hbar\dot{\theta}/2e. \tag{2.2}$$

Here θ is the quantum phase difference between the superconducting pair wavefunctions on both sides of the junction. The first term on the right-hand side in (2.1) is the super current due to the tunnelling of the pairs while the second term is the contribution from quasiparticles. The cos θ term is the phase-dependent part of the quasiparticle current, which has no effect on the RF induced steps or the I–V characteristics and as such will not be further considered in this paper.

A simple model for the junction is the Josephson element shunted by a capacitance C and resistance R. When driven by a constant DC bias i_{DC} and a periodic current of frequency ω the equation for the junction is (Pedersen and Saermark 1973)

$$C(\mathrm{d}v/\mathrm{d}t) + v/R + i_1 \sin\theta = i_{DC} + i_f \sin\omega t. \tag{2.3}$$

The quasiparticle current $i_2 = v/R$. Further choosing the resistance R to depend on v as

$$R = \hbar\gamma/2ev \tag{2.4}$$

where γ is a constant, we define the following dimensionless parameters:

$$I = i_{DC}/i_1 \qquad A = i_f/i_1 \qquad k = (\gamma C)^{-1}. \tag{2.5}$$

The time t is redefined as $\omega_j t$ where ω_j is the Josephson plasma frequency given by

$$\omega_j = (2ei_1/\hbar C)^{1/2} \tag{2.6}$$

Then (2.3) together with (2.2) gives us

$$\ddot{\theta} + k|\dot{\theta}|\dot{\theta} + \sin\theta = I + A\sin\omega t. \tag{2.7}$$

Written this way, this equation can model interesting physical situations such as a perturbed pendulum with quadratic damping. Throughout the paper we invoke the

pendulum analogy quite often, to clarify the nature of the different possible modes of the system. When $A = 0$, the DC characteristics of the junction consist of a zero-voltage branch corresponding to the oscillatory modes of the pendulum and a non-zero-voltage branch, arising from the running or rotational modes. When $A \neq 0$, we get a series of steps where $\langle v \rangle$ is locked to the rational multiples of the driving frequency ω. The chaotic states are due to the random jumps between different steps and this intermittent type of chaos is the one that is usually observed in experiments.

3. Parameter space analysis

An overall picture of the occurrence of the periodic and chaotic states in the system can be understood from a parameter space plot of the problem. The parameter space in this context is (k, I, A, ω). For the time being we consider the zero-bias situation, the effect of I being dealt with separately. Moreover, we consider a case of low damping and keep $k = 0.1$ throughout. Thus the parameter space reduces to the plane (A, ω). For our numerical analysis, (2.7) is considered as a three-dimensional dissipative system in $(\theta, \dot{\theta}, \omega t)$. For each set of values (A, ω), (2.7) is integrated using a fourth-order Runge–Kutta algorithm and the asymptotic states are identified by plotting the phase portraits in the $(\theta, \dot{\theta})$ plane and the Poincaré maps in sections at a specified phase of the driving term. The power spectrum computed using the fast Fourier transform (FFT) (Higgins 1976) is also employed to get an idea about the number of frequencies involved and to identify the truly chaotic states. For one value of ω, A is slowly varied and a bifurcation diagram is drawn by plotting $\dot{\theta}$ $(=2ev/\hbar)$ values, sampled at frequency ω, against A. The first thousand values are discarded as transient and next thousand are plotted. A uniform line in this diagram would correspond to a window of stable periodic resonance mode while scattered random points would imply chaotic regions. The period doubling bifurcations, if any, can also be clearly seen. Observing the phase portraits and the Poincaré maps side by side, we fix the details of the dynamics of the system in the parameter space. This is repeated changing ω by 0.05. Thus the parameter space plots given in figure 1 are drawn.

In figure 1, the region below the curves C_1 and C_2 leads to asymptotically stable periodic modes with $\langle \dot{\theta} \rangle = 0$. These symmetric modes form the zero-voltage branch of the junction. Above these curves, however, irregular and random behaviour can be seen. The transition curves are drawn by calculating the Lyapunov characteristic exponent (LCE) which gives the average rate of divergence or convergence of two initially close trajectories. In the periodic region, the LCE is negative, while in the chaotic region at least one LCE is greater than zero. So we compute the maximum LCE throughout the (A, ω) plane in steps of (0.05, 0.05), following the conventional procedure (Wolf *et al* 1985). Here the first 2000 values are discarded and LCE is calculated using the next 2000 values.

The period doubling region occurs only on the high-frequency side (marked by stripes in figure 1). The reason for this will be made clear in section 4. The dotted region corresponds to states of mild chaos associated with rotational or non-zero-voltage branches that are of broken symmetry. In this region, even when the voltage is locked to a harmonic of ω, the LCE value is positive and hence is called a state of locked chaos. Similar behaviour has been observed experimentally on junctions of the Pb–Te–Pb type (Octavio and Nasser 1984) where the equivalent noise temperature is found to rise even before the voltage unlocks. States of locked and unlocked chaos have been mentioned

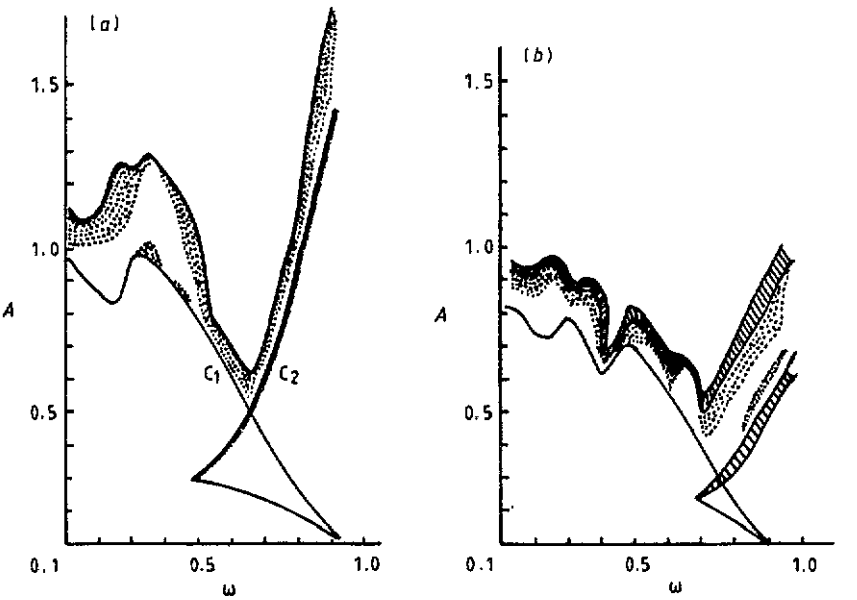

Figure 1. Parameter space plot of the QRSJ model with $k = 0.1$. The curves C_1 and C_2 represent transition from periodic to chaotic regions. The period doubling scenario occurs in the striped regions while the dotted regions show locked chaos in the non-zero-voltage branches: (a) with no DC bias and (*b*) with $I = 0.2$ V.

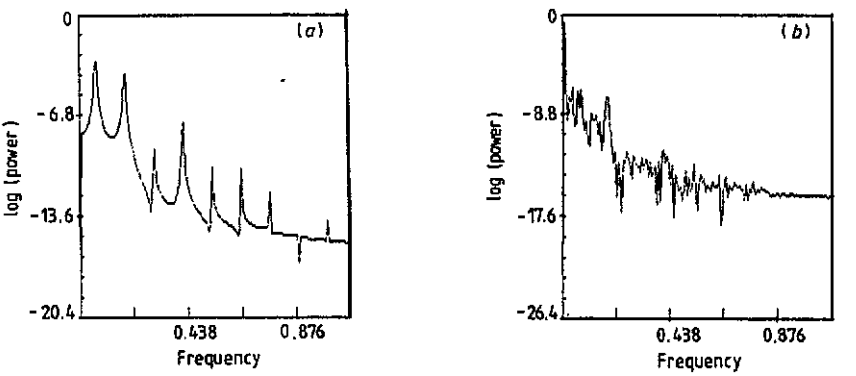

Figure 2. Power spectra of the states with log (power) plotted along the *y* axis and frequency along the *x* axis. Here $\omega = 0.55$ and $k = 0.1$: (*a*) locked chaos at $A = 0.7$ and (*b*) unlocked chaos at $A = 0.825$.

earlier in the work of Xiao and Yao (1989). Our results also indicate that in the state of locked chaos the LCE value is small (about 10^{-2}) but positive and the FFT shows, in addition to the fundamental, a few peaks that correspond to the harmonics of ω and their subharmonics. However in the unlocked chaotic regions, the LCE is large and positive and the FFT displays a large number of peaks together with broad brands. These are shown in figure 2.

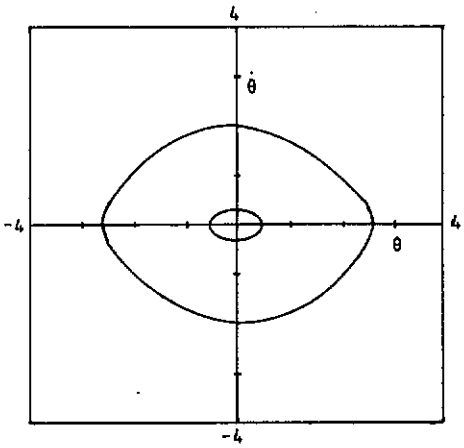

Figure 3. Stable periodic limit cycles LC1 and LC2 of the zero-voltage type with $\omega = 0.6, k = 0.1, I = 0$ and $A = 0.3$. The initial value chosen for LC1 is (0, 1) while that for LC2 is (−2.4, −0.5).

The pattern of behaviour is significantly altered by the application of a small DC bias, say $I = 0.2$ V (figure 1(*b*)). This, first of all, introduces a symmetry breaking in the system which makes period doubling occur earlier. The transition to chaos for low ω values is not much affected, the only change being that chaos sets in for lower values of A. The states with locked chaos also occur earlier. On the high-frequency side, the period doubling region is broader and is brought down to much lower A values.

4. Stable periodic modes

Considering the damping and the driving terms as perturbations, we can see that the unperturbed system with $I = 0$ corresponds to a simple pendulum and the possible dynamic states in the phase space $(\theta, \dot{\theta})$ are the oscillatory modes and rotational modes with the separatrix orbit in between. With damping, the stable and unstable parts of the separatrix separate out and the asymptotic states or attractors are stable fixed points or centres at $(2n\pi, 0)$ and unstable fixed points or saddles at $((2n + 1)\pi, 0)$ where $n = 0, \pm 1, \pm 2, \pm 3 \ldots$. The centres and saddles thus alternate along the θ axis and correspond to the potential minima and maxima. For small values of A and ω, the system describes simple limit-cycle-like orbits inside the wells.

On the low-frequency side, the asymptotic state continues to be a small-amplitude motion of the oscillatory type referred to as LC1, until transition to chaos takes place. As ω increases, the system is able to support another large-amplitude resonance mode, LC2. While LC1 is stable on the left-hand side of the curve C_1, LC2 is stable on the right-hand side of the curve C_2 (figure 1(*a*)). There is a small triangular region where LC1 and LC2 coexist with hysteresis. Figure 3 shows these two modes for the same values of A and ω but for different initial conditions. The obvious difference between them is that LC1 is a small-amplitude oscillation deep inside the potential well while LC2 is a large-amplitude oscillation near the top of the well. They have different basins of attraction, that is the sets of initial points that evolve into LC1 and LC2 are different, with a boundary separating them. This can be seen clearly in figure 4. Moreover, they follow two different routes to chaos as A increases. While LC2 prefers the period doubling route, LC1 disappears via an entirely different mechanism. This will be made more explicit in section 5. In this context, we would like to add that such modes have been reported in some earlier work in the

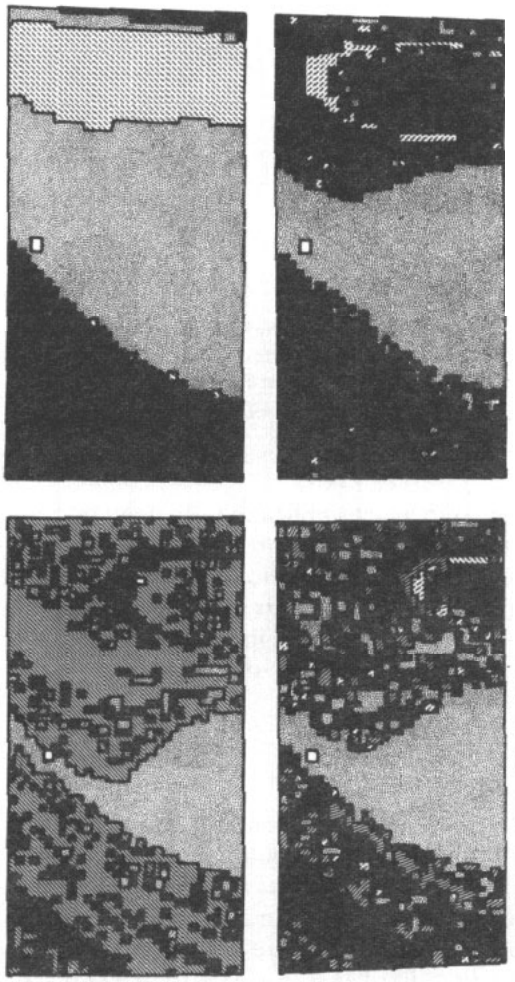

Figure 4. Evolution of basin boundaries corresponding to the two modes LC1 and LC2 at $\omega = 0.6$ and $k = 0.1$. The region of phase space considered is 0 to 3 along the θ axis and -3 to 3 in the $\dot{\theta}$ direction. Starting from the upper left-hand figure, the A values in the clockwise direction are 0.3, 0.35, 0.406, 0.45. Here the dotted areas correspond to the basin of LC1 while the broken-hashed regions represent that of LC2. The hashed regions end up in rotational modes while the dark region marks points that lead to limit cycles in other potential wells. The white dot in the dotted region refers to the Poincaré map of LC1.

usual RSJ model (Beasley and Huberman 1982) even though details regarding the transition to chaos are not available.

However, regular periodic states corresponding to non-zero-voltage steps, with the voltage locked to a multiple of ω do not appear to be asymptotically stable states in our system. In the RSJ model with linear damping, rotational modes with phase locking have been observed (D'Humieres *et al* 1982). When the damping is quadratic in $\dot{\theta}$, the dependence of the damping factor on $\dot{\theta}$ introduces a sort of feedback in the system, since, at each stage, damping varies with $\dot{\theta}$. So rotational modes with large $\dot{\theta}$ values are soon damped to oscillatory modes or end up in states with a certain randomness that do not settle down to exactly periodic locked states.

5. Crisis and chaos

As has been mentioned earlier, the transition to chaos in the parameter space is fixed by studying the LCE values and the bifurcation diagrams. We find that, on the low-frequency

side, say up to $\omega = 0.65$, chaos sets in through LC1. Nevertheless, LC1 does not show any tendency to period-double, even in the presence of a DC bias. The disappearance of LC1 is via a reverse-tangent bifurcation or saddle-node bifurcation where it meets its unstable counterpart, bringing about mutual destruction (Xiao and Yao 1989). Just before this happens, the unstable cycle can collide with the boundary of the chaotic attractor existing for higher values of A. This will result in the sudden disappearance of chaos, leaving only chaotic transients. Although we have no direct numerical evidence for this collision at this stage, to the extent that we have been able to establish, we can say that the transition is very sudden, the LCE becoming positive within a very small change in $A \approx 10^{-4}$. By studying the transients very close to the transition value, the course of events is obviously the periodic limit cycle → chaotic transients → chaos. Such a scenario has been named a reverse boundary crisis in the literature (Grebogi *et al* 1983). We illustrate this in figure 5(*a*) for $\omega = 0.3$ where $A_c = 1.017$. The average lifetime of the transients $\langle \tau \rangle$ should follow a scaling law $|a - a_c|^{\nu}$, where A_c is the transition value. Detailed computations to evaluate this scale factor ν for the present problem are underway and the results will be made available in a subsequent paper.

For ω values lying in the triangular region, we find that, before LC1 disappears, LC2 is produced by a saddle-node bifurcation. This undergoes period doubling as A increases, resulting in a chaotic attractor, which disappears via a boundary crisis. The numerical study of the evolution of the basin boundaries near the crisis region is shown in figure 4. Here in the first part with $A = 0.3$, LC1 and LC2 are stable and their boundaries are shown separately. As A increases, the basin of LC2 changes shape drastically and disappears beyond the crisis point. LC1 still continues as the asymptotic state of the system until chaos sets in. As A increases further, rotational modes with locked chaos are produced. They undergo period doubling followed by an interior crisis, where the unstable modes collide with the period-doubled attractors inside their basins, resulting in a sudden expansion of the attractor size. As this happens, there is a merging of the different basins. The evolution of the boundaries during an interior crisis has been studied in detail earlier in related systems (Gwinn and Westervelt 1985) and hence is not included here. The transition scenario for $\omega = 0.55$ clearly illustrates this sequence of events in figure 5(*b*).

For $\omega > 0.65$, chaos sets in through LC2 and hence the mechanism is the period doubling cascade. For higher values of A, rotational modes undergo period doubling and interior crisis to reach chaos. The LCE values in this region vary gradually with A and become positive even before the LC2 period doubles. This is because of a heteroclinic tangle formed by the unstable and stable branches of the different separatrices. Two initial conditions, differing by very small values, end up asymptotically in widely separated potential wells. This would mean that the basin boundaries, separating the states inside different wells, have a fractal nature and even though the system is asymptotically attracted to a periodic state, there is an uncertainty regarding the final state. This is a feature common to non-linear systems with multiple attractors (Li and Moon 1990, Thompson and Soliman 1991) and though the situation is not exactly chaotic in the strict sense of the word, it certainly heralds chaos in the system. In addition, this region is most affected by the presence of a DC bias in the junction. This should be clear by comparing the bifurcation diagrams given in figure 6.

6. Concluding remarks

In this work, an exposition of the various possible dynamical states of QRSJ is made, with special emphasis on the pattern of behaviour during onset of chaos. It is found that on

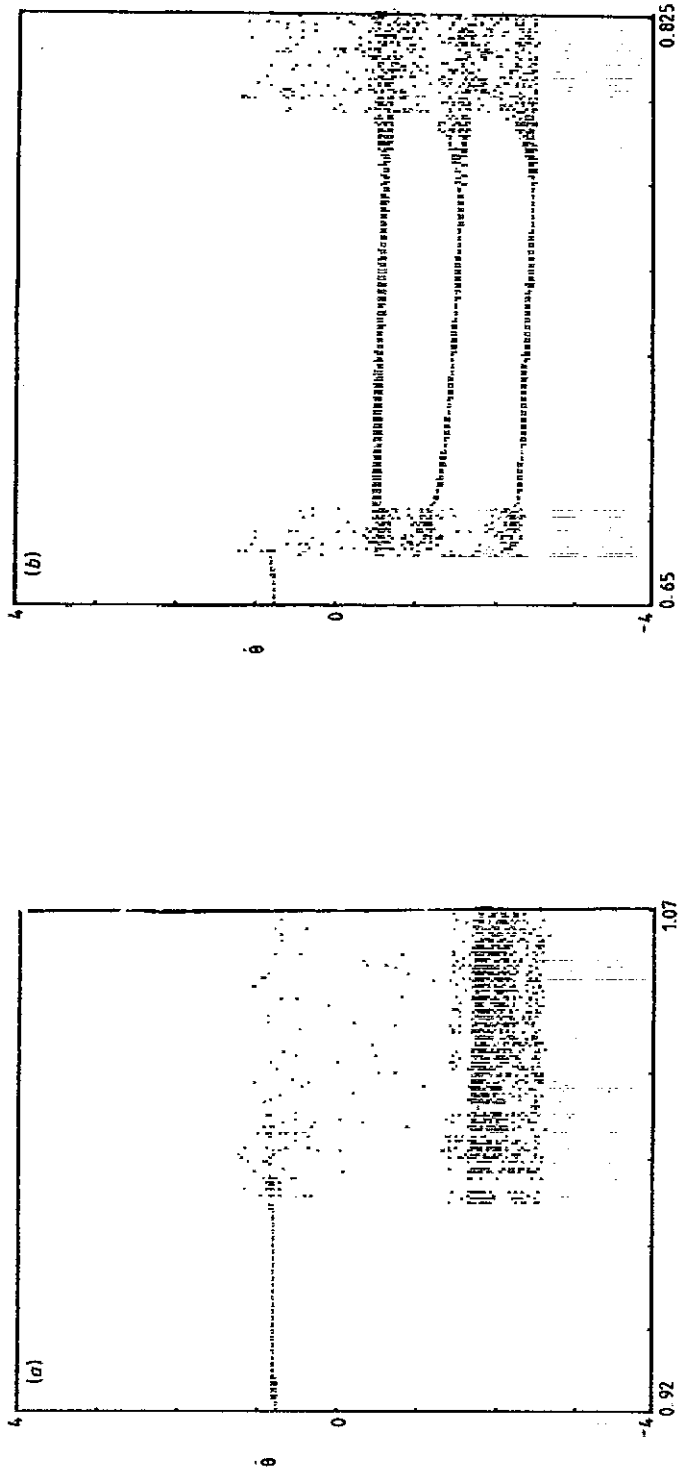

Figure 5. Bifurcation diagrams in which $\dot{\theta}$ values sampled at ω are plotted against A. (*a*) For $\omega = 0.3$, the limit cycle LC1 disappears through a reverse boundary crisis at $A_c = 1.017$. (*b*) At $\omega = 0.55$, rotational modes with locked chaos at frequencies $\omega/3$ are seen and they undergo period doubling followed by an interior crisis at $A = 0.782$, resulting in unlocked chaos in the system.

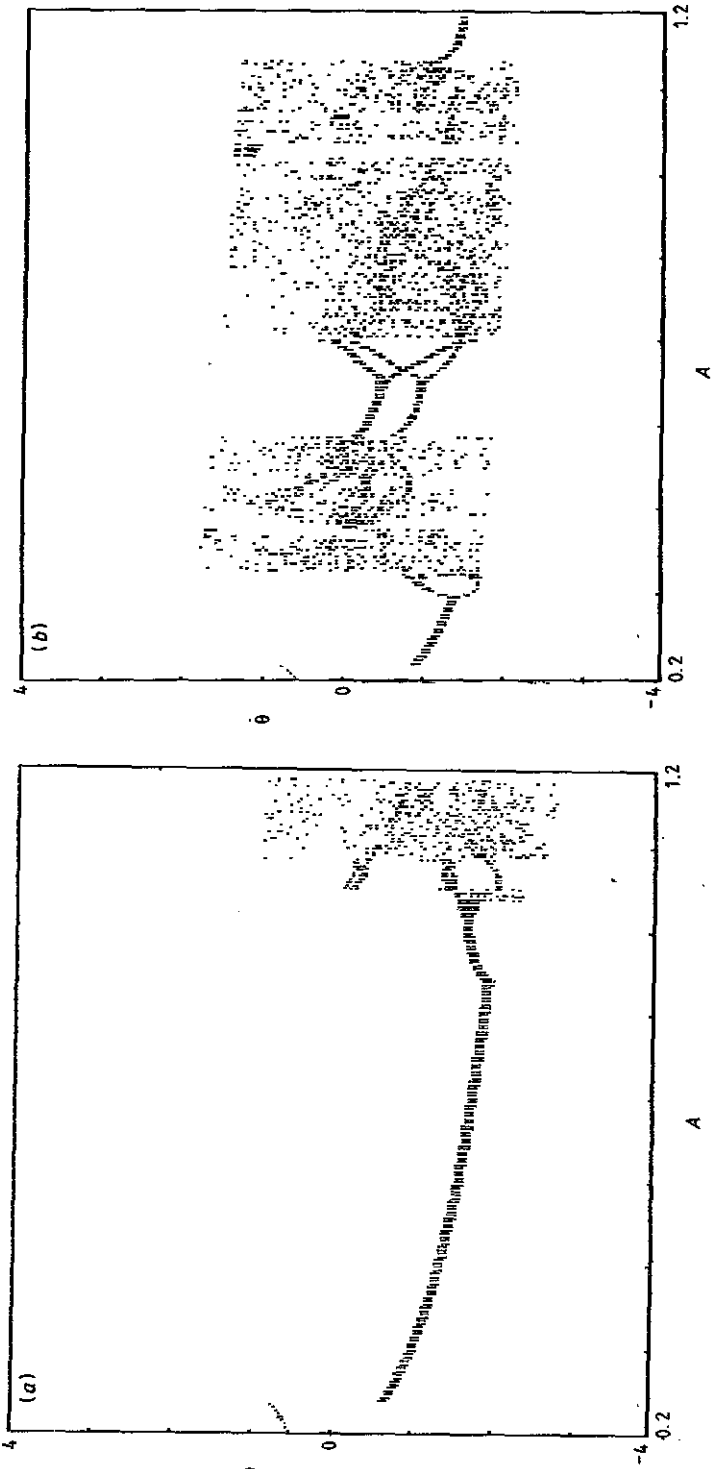

Figure 6. The effect of a DC bias in the bifurcation structure for $\omega = 0.8$ and $k = 0.1$. (*a*) With no DC bias, period doubling occurs only at $A = 0.962$. (*b*) With DC bias, $I = 0.2$ V, period doubling starts at $A = 0.314$.

the low-frequency side, chaos is brought in by a reverse boundary crisis while on the high-frequency side, it is due to interior crisis preceded by a period-doubling scenario.

The present model set against the usual RSJ brings out the following interesting points. In the RSJ model, for low values of ω, chaos occurs later compared to QRSJ. Moreover, the chaotic state runs over larger values of $\dot{\theta}$. Phase-locked running modes have been observed in RSJ, but in our model such locked states have positive LCE values. However, direct experimental measurements under identical conditions are not available at present and therefore it is difficult to comment on the superiority of either model in explaining experimental observations. One obvious fact is of course that QRSJ takes into account the non-linear nature of the I–V curves and as such is a better fit for the actual junction. However, a striking discrepancy between experimental observations and the numerical results is that so far chaos has been observed experimentally only in the presence of DC bias (Octavio 1990). Our model also does not explain this but we find that the periodic modes continue to be stable even for large values of A and are quite reluctant to period-double when there is no DC bias. The DC bias makes period doubling occur much earlier and chaos sets in for much smaller values of A.

Acknowledgments

The author wishes to thank the CSIR, New Delhi for financial support through a research associateship.

References

Ambika G 1990 *Phys. Lett.* A **150** 273
Ambika G and Babu Joseph K 1990 *Symmetries and Singularity Structures—Integrability and Chaos in Nonlinear Dynamical Systems* ed M Lakshmanan and M Daniel (Heidelberg: Springer) p 196
Ambika G, Babu Joseph K and Nandakumaran V M 1991 *Mod. Phys. Lett.* B **5** 519; Errata *Mod. Phys. Lett.* B **5** 1037
Bartuccelli M, Christiansen P L, Pedersen N F and Sørenson M P 1986 *Phys. Rev.* B **33** 4686
Beasley M R and Huberman B A 1982 *Comment. Solid State Phys.* **10** 155
Cicogna G 1987 *Phys. Lett.* A **121** 403
—— 1988 *Phys. Lett.* A **131** 98
D'Humieres D, Beasley M R, Huberman B A and Liebhaber A 1982 *Phys. Rev.* A **26** 3483
Grebogi C, Ott E and Yorke J A 1983 *Physica* D **7** 181
Gwinn E G and Westervelt R M 1985 *Phys. Rev. Lett.* **54** 1613
—— 1986 *Phys. Rev.* A **33** 4143
Harris R E 1974 *Phys. Rev.* B **10** 84
Higgins R J 1976 *Am. J. Phys.* **44** 766
Huberman B A and Crutchfield J P 1979 *Phys. Rev. Lett.* **43** 1743
Huberman B A, Crutchfield J P and Packard N H 1980 *Appl. Phys. Lett.* **37** 750
Iansiti M, Hu Q, Westervelt R M and Tinkham M 1985 *Phys. Rev. Lett.* **55** 746
Jing Z J 1989 *SIAM J. Appl. Math.* **49** 1749
Kautz R L and Monaco R 1985 *J. Appl. Phys.* **57** 875
Li G X and Moon F C 1990 *J. Sound Vib.* **136** 17
Octavio M 1990 *Physica* A **163** 248
Octavio M and Nasser C R 1984 *Phys. Rev.* B **30** 1586
Pedersen N F and Saermark K 1973 *Physica* **69** 572
Thompson J M T and Soliman M S 1991 *Proc. R. Soc. A* **432** 101
Wolf A, Switt J, Swinney H and Vastano J 1985 *Physica* D **16** 285
Xiao W and Yao X 1989 *Act. Phys. Sin.* **38** 137
Yao X, Wu J Z and Ting C S 1990 *Phys. Rev.* B **42** 344